Fixed number of segments in unidirectional decompositions of fluence matrices for step-and-shoot IMRT

2011 Phys. Med. Biol. 56 2601

(http://iopscience.iop.org/0031-9155/56/8/017)

Phys. Med. Biol. **56** (2011) 2601–2615 doi:10.1088/0031-9155/56/8/017

Fixed number of segments in unidirectional decompositions of fluence matrices for step-and-shoot IMRT

X Mellado[1], J M Artacho[1,4], M Hernández[2], S Cruz[1] and E Millán[3]

[1] Communications Technology Group (GTC), Aragón Institute for Engineering Research (I3A), Universidad de Zaragoza, C/ María de Luna 1, 50018 Zaragoza, Spain
[2] Computer Science and Systems Department (DIIS), Aragón Institute for Engineering Research (I3A), Universidad de Zaragoza, C/ María de Luna 1, 50018 Zaragoza, Spain
[3] Physics and Radiological Protection Service, Hospital Clínico Universitario Lozano Blesa, Avenida San Juan Bosco, 15, 50009 Zaragoza, Spain

E-mail: xme@unizar.es, jartacho@unizar.es, mhg@unizar.es, cruzll@unizar.es and emillan@salud.aragon.es

Received 6 August 2010, in final form 28 February 2011
Published 28 March 2011
Online at stacks.iop.org/PMB/56/2601

Abstract

The decomposition of a fluence matrix in step-and-shoot mode for intensity-modulated radiation therapy (IMRT) usually yields a large number of segments (NS) and, consequently, treatment time is substantially increased. In this paper, we propose a method for reducing the original NS in multileaf collimator segmentations to a user-specified quantity. The proposed method clusters original segments into the same number of groups as desired NS, and computes for each group an equivalent segment and an associated weight. In order to avoid important changes in dose–volume histograms (DVHs), equivalent segments and weights are computed taking into account the original fluence matrix and preserving the highest fluence zones, thus staying as close as possible to the original planned radiation. The method is applicable to unidirectional segmentations, where there is no backtracking of leaves, since this property facilitates the grouping of segments. The experiments showed that treatment times can be considerably reduced, while maintaining similar DVHs and dosimetric indexes. Furthermore, the algorithm achieved an excellent reduction/dose-quality ratio since the final NS was close to that reported for direct step-and-shoot solutions.

[4] Author to whom any correspondence should be addressed.

1. Introduction

Step-and-shoot (or static) mode in intensity-modulated radiation therapy (IMRT) was originally devised with an optimization phase for planning the dose to be delivered by each beam as a fluence matrix, and a segmentation phase for decomposing this matrix into a feasible set of multileaf collimator (MLC) segments (Galvin *et al* 1993). One known drawback of this approach is that optimization algorithms often generate very heterogeneous fluence matrices (Spirou *et al* 2001, p 2105), whose corresponding segmentations yield large number of segments (NS) and large total number of monitor units (TNMU), and consequently treatment time is substantially increased (Shepard *et al* 2002, p 1007).

This drawback has been overcome with techniques that process fluence matrix values such as smoothing (Webb *et al* 1998, Alber and Nüsslin 2000, Spirou *et al* 2001, Matuszak *et al* 2007), clustering (Bär *et al* 2001, Wu *et al* 2001) or segmentation-driven smoothing (Mellado *et al* 2010). However, the results of previous methods in terms of delivery efficiency have been surpassed by direct step-and-shoot (DSS) solutions such as direct aperture optimization (Shepard *et al* 2002), direct machine parameter optimization (Löf and Rehbinder 2002, Hårdemark *et al* 2003) or graph-based aperture optimization (Carlsson 2008). These approaches combine optimization and segmentation into a single phase by directly optimizing MLC leaf positions instead of fluence matrices. Their efficiency derives from the fact that the NS can be *a priori* fixed and, as a consequence, treatment time and complexity can be considerably reduced.

Methods with the ability of fixing the NS are advantageous, since the plans obtained are simple with compact and large apertures, bigger associated weights, but fewer TNMU than two-phase plans. This reduction in complexity allows (1) obtaining a short treatment time, thus patient comfort as well as throughput of patients can be improved; (2) decreasing leakage exposure, that reduces the risk of collateral effects and radiation-induced secondary cancers (Romeijn *et al* 2005, Carlsson 2008, Broderick *et al* 2009), and (3) obtaining a plan that is easier to deliver (Sharpe *et al* 2000, p 2719). For all these reasons, the possibility of *a priori* fixing the NS would be highly desirable in two-phase step-and-shoot IMRT.

In this work, we propose a method for post-processing MLC segmentations that can be included in two-phase step-and-shoot IMRT treatment planning systems and allows us to *a priori* fix the NS. This method is applicable to unidirectional MLC segmentations (Siochi 1999, Artacho *et al* 2009), where leaves are moved in a single direction. Unidirectional leaf movement makes these segmentations very suitable inputs for our method, since the leaf arrangement provides highly correlated adjacent segments, as can be seen in figure 1. This facilitates their clustering into the same number of groups as desired NS, so as to generate for each group an equivalent segment and an associated weight, which is the basic idea of our method. In order to avoid substantial changes in dose–volume histograms (DVHs), equivalent segments and their weights are computed taking into account the original fluence matrix and preserving the highest fluence zones, thus staying as close as possible to the original planned radiation. As reported in the experimental section, the proposed method has been shown to achieve an excellent reduction/dose-quality ratio since the method was able to reduce the original NS up to 75% without compromising plan quality.

This paper is organized as follows. In section 2, we describe the proposed method, the experimental setup and the clinical cases used in section 3, where we present the numerical results, including treatment time measurements. Finally, the discussion and conclusions are presented in sections 4 and 5, respectively.

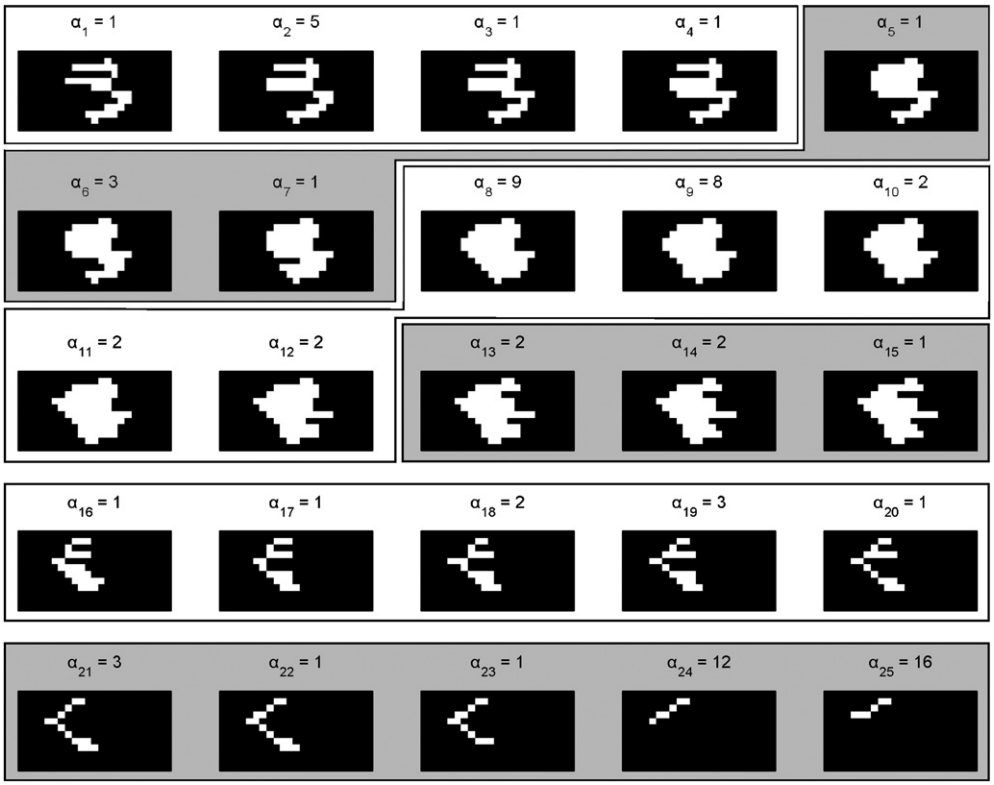

Figure 1. Fluence matrix segmentation of one beam from a prostate case with 25 segments, clustered into six groups. The final grouping is 4-3-5-3-5-5, whereas the initial grouping was 4-4-4-4-4-5.

2. Method and materials

The proposed method uses as input the decomposition of a fluence matrix, independently obtained by one of the unidirectional segmentation methods proposed in the literature such as Siochi (1999) or Artacho *et al* (2009), and the number of desired segments. The decomposition, or segmentation, of an $M \times N$ fluence matrix A is defined as a set of pairs composed of an aperture (segment) plus an associated weight accounting for a relative beam-on time, $(S_k, \alpha_k)_{1 \leqslant k \leqslant K}$, in such a way that

$$A = \sum_{k=1}^{K} \alpha_k \cdot S_k \tag{1}$$

where K is the NS and $k \in [1, \ldots, K]$ is the index representing the segment position in the original segmentation. Each segment S_k is a binary matrix with the same dimensions as the fluence matrix A. When a given position in the segment is equal to 0, this position is covered by a leaf. When it is equal to 1, the position allows radiation to pass. The segments are also subject to some constraints. In this work, we will consider one aperture per row and avoid interleaf collision (Siochi 1999, p 672).

In our method, the processing of the original segmentation is divided into four steps. First, the original segments are clustered into as many groups as desired segments. Second,

an equivalent segment S^{eq} is generated for each group. Third, an associated weight α^{eq} is computed for each equivalent segment. These equivalent segments and weights are intended to obtain an approximation of the original segmentation in order to provide a simpler plan with similar quality

$$A = \sum_{k=1}^{K} \alpha_k \cdot S_k \approx \sum_{g=1}^{G} \alpha_g^{eq} \cdot S_g^{eq} \tag{2}$$

where G is the number of desired segments and $g \in [1, \ldots, G]$ is the index representing the segment position in the processed segmentation. Finally, for each equivalent segment, it is checked in the overlap region with posterior segments that the fluence accumulated does not exceed that originally planned in matrix A. Otherwise, the posterior segments are modified to fulfil this requirement. These steps are detailed in the following subsections.

2.1. Clustering the original segments into groups

The first step of our method consists of clustering the original segments from a fluence matrix decomposition into the same number of groups as the desired NS. Grouping is driven by similarity among the segments. To this end, we define the correlation between two segments S_1 and S_2 as

$$\sigma = \frac{\sum_{i=1}^{M} \sum_{j=1}^{N} (S_1(i, j) \wedge S_2(i, j))}{\max\left(\sum_{i=1}^{M} \sum_{j=1}^{N} S_1(i, j)\ ,\ \sum_{i=1}^{M} \sum_{j=1}^{N} S_2(i, j)\right)}. \tag{3}$$

Thus, σ accounts for the overlap between both segments and their relative size. The $i \in [1, \ldots, M]$ and $j \in [1, \ldots, N]$ indexes are used to move through the rows and columns, respectively, of the fluence matrix or the original segment. The clustering procedure takes advantage of the similarity among adjacent segments in unidirectional segmentations measured by this correlation coefficient as follows.

First, clusters are uniformly initialized as groups of length round(K/G). Second, for each group it is checked whether the last segment is more closely correlated (using equation (3)) with the previous segment in this group or with the first segment in the next group. In the latter case, it becomes part of the next group. Otherwise, the same test is applied to the first segment in the next group, in order to check whether it should become part of the current group. This exchange process is iteratively applied, allowing multiple changes while controlling group cardinalities. One or two iterations are usually enough to increase internal group correlation and exchange segments that were incorrectly assigned during cluster initialization. This number of iterations is intended to keep a balance between intergroup cardinality and intragroup correlation, thus avoiding groups with a relatively small NS. A very unbalanced distribution of segments would make some groups much larger than others and more difficult to represent with a single aperture, since the difference between the first segment and the last one may be considerable.

As an example, two iterations of the proposed procedure were applied to a fluence matrix segmentation of a prostate case with 25 segments clustered into six groups. The result is shown in figure 1.

2.2. Computing equivalent segments

After clustering, an equivalent segment S^{eq} is computed for each group of segments. This computation is a weighted sum driven by the original fluence matrix values, in such a way that the equivalent segment shape will contain those leaf apertures that contribute to high radiation

regions. Thus, the complexity of the segmentation is reduced, while keeping the delivered radiation as close as possible to the original planned one.

The weighted sum is based on the fact that the highest fluence values correspond to beamlets that radiate only a CTV, which should be included and not modified in the equivalent segment in order not to degrade the plan quality, whereas the lowest fluence values correspond to beamlets that radiate CTV and OAR at the same time, which are allowed to be modified or even excluded from the equivalent segment. Therefore, we define a weighting matrix W of size $M \times K$ in order to compute equivalent segments, where each column contains the sum of the original fluence values in each row between the left and right leaves denoted by l_k and r_k, respectively, for the kth segment

$$W(i,k) = \sum_{j=l_k(i)+1}^{r_k(i)} A(i,j) \tag{4}$$

$$0 \leqslant l_k(i) \leqslant r_k(i) \leqslant N$$

$$i \in [1,\ldots,M],\ k \in [1,\ldots,K] \tag{5}$$

where positions $l_k(i) + 1$–$r_k(i)$ are exposed to radiation, and the left leaf at positions $[0,\ldots,l_k(i)]$ and the right leaf at positions $[(r_k(i)+1),\ldots,N]$ are blocking radiation. The case of a row totally closed is included as $l_k(i) = r_k(i)$.

When equivalent segments are computed, the corresponding leaves do not often match the beamlet positions. This is intensified by the use of a weighting matrix. Accordingly, it is necessary to redefine the segment representation used in equation (1) in order to deal with continuous leaf positions. Thus, the S_k segment is now represented as an $M \times 2$ matrix of real numbers $S_k^{'}$, where the first column contains the left leaf location l_k and the second column contains the right leaf location r_k. From here on, any entity related to continuous leaf positions will be followed by an apostrophe $'$. This change of representation is illustrated in example 2 of the appendix. It should be noted that, although the step-and-shoot mode uses discrete leaf positions defined by the beamlets, this is not an MLC limitation, since the MLC is able to place leaves in continuous positions. Taking advantage of this feature, our method allows placing the leaves in any position even though this position does not match the horizontal discretization of the rows.

Using this new representation $S^{'}$ for segments with continuous leaf positions, the generation of equivalent segment $S^{\mathrm{eq}'}$ is performed by computing for all the leaves belonging to open rows

$$S_g^{\mathrm{eq}'}(i,x) = \frac{\sum_{k=u_g}^{v_g}(W(i,k)\cdot S_k^{'}(i,x))}{\sum_{k=u_g}^{v_g} W(i,k)} \tag{6}$$

$$g \in [1,\ldots,G], i \in [1,\ldots,M],\ x \in [1,2],\ u_g, v_g \in [1,\ldots,K]$$

where $u_g, v_g \in [1,\ldots,K]$, and $u_g \leqslant v_g$, are the indexes in the original segmentation of the first and last segments for the gth group, respectively, and $x \in [1,2]$ is used to specify the leaf bank (left or right) of an MLC.

The final step is to ensure that $S^{\mathrm{eq}'}$ is a feasible segment for the MLC used, otherwise it should be modified to meet the MLC constraints. In our current approach, one aperture per row is automatically generated in equation (6). Therefore, only the interleaf collision constraint is imposed by opening any pair of offending leaves until there is no collision. The whole process of computing an equivalent segment is illustrated in examples 1 and 2 of the appendix.

2.3. Computing associated weights

The weight associated with an equivalent segment, $\alpha^{eq'}$, is generated by accumulating the fluence delivered by the original group of segments and achieving a uniform delivery with the new equivalent segment area. For this purpose, we define the cumulative fluence matrix A_g^{cu} of a group as the accumulation of the different segments previously multiplied by their corresponding weights

$$\begin{aligned} &A_g^{cu} = \sum_{i=u_g}^{v_g} \alpha_i \cdot S_i \\ &u_g, v_g \in [1, \ldots, K], \ g \in [1, \ldots, G]. \end{aligned} \tag{7}$$

Thus, A_g^{cu} represents the contribution of the gth group to the fluence matrix A. Then, we define the weight β_g' as the sum of the old fluence delivered by the group divided by the new equivalent segment area

$$\begin{aligned} &\beta_g' = \frac{\sum_{i=1}^{M}\sum_{j=1}^{N} A_g^{cu}(i,j)}{\sum_{i=1}^{M}\left(S_g^{eq'}(i,2) - S_g^{eq'}(i,1)\right)} \\ &g \in [1, \ldots, G] \end{aligned} \tag{8}$$

which is truncated to the maximum value found in A_g^{cu}, in order to prevent an overdose caused by a shrinking of the $S^{eq'}$ area compared to the original A_g^{cu} area, yielding

$$\begin{aligned} &\alpha_g^{eq'} = \max\left(\beta_g', \max_{i=1}^{M}\left(\max_{j=1}^{N}\left(A_g^{cu}(i,j)\right)\right)\right) \\ &g \in [1, \ldots, G]. \end{aligned} \tag{9}$$

2.4. Checking the equivalent segment overlapping

Once equivalent segments and weights are computed, it remains to be checked that there is no region where several equivalent segments overlap and the fluence accumulated is higher than that originally planned in matrix A. In these cases, the spatial location and delivery order of the segments are used for solving this situation.

Let $S_1^{eq'}$ be the first equivalent segment obtained from an unidirectional segmentation in left-to-right direction. If there is an overlapping area with $S_2^{eq'}$, where $\alpha_1^{eq'} + \alpha_2^{eq'}$ exceeds the fluence planned, this situation is detected and fixed as follows. For each row $i \in [1, \ldots, M]$ in $S_1^{eq'}$ with open leaves, the condition for overlapping is that $S_2^{eq'}(i,1)$ is smaller than $S_1^{eq'}(i,2)$. In this case, if the fluence added by $\alpha_2^{eq'}$ to $\alpha_1^{eq'}$ exceeds the maximum fluence value found in the original fluence matrix between both leaves, then $S_2^{eq'}(i,1)$ is moved forward until it reaches the location of $S_1^{eq'}(i,2)$. Figure 2 illustrates this example. The process has to be repeated comparing each segment with all the next ones until there is no overlapping.

2.5. Data and experimental setup

The experiments reported in this paper were performed using (1) clinical cases planned with the PCRT 3D® (Técnicas Radiofísicas, S.L. C/Gil de Jasa, 18E, 50006 Zaragoza, Spain, www.trf.es) treatment planning system, (2) two different unidirectional segmentation methods rod pushing (RP) (Siochi 1999) and OTNMU (Artacho *et al* 2009, p 577) and (3) a Siemens ONCOR™ linear accelerator with an Optifocus™ MLC for obtaining beam delivery times.

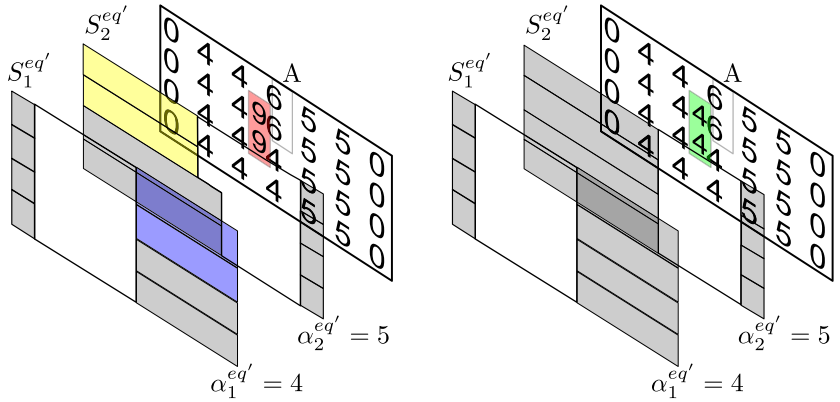

(a) Initial solution. (b) Overlap checking done.

Figure 2. Overlap checking example with two equivalent segments. *A* is the original fluence matrix. The right leaves $S_1^{eq'}(1, 2)$ and $S_1^{eq'}(2, 2)$ (in blue) will respectively cause the left leaves $S_2^{eq'}(1, 1)$ and $S_2^{eq'}(2, 1)$ (in yellow) to move forward in order to avoid the delivery of 9 MU instead of the original 6 MU.

Results were obtained under the following conditions: (1) the constraints used for Siemens MLC were one aperture per row and interleaf collision, (2) unidirectional segmentations were performed from left to right and from right to left and the best solution was selected and (3) unless otherwise stated, the applied reduction was one equivalent segment for each four original ones (4:1)[5], in order to have a good reduction ratio without considerably modifying the original DVHs. This condition was applied to all beams, independently of any criteria such as CTV and OAR positions, initial NS or fluence matrix heterogeneity. However, it is possible to fix for each beam a different reduction ratio. (4) The number of iterations used for exchanging segments while clustering into groups was 2, and (5) all plans were generated with a photon energy of 6 MV for each patient and normalized so as the mean dose of the main target volume contour is equal to the prescribed dose.

We present detailed results achieved by the method in three clinical cases. The first case is a prostate cancer radiated from five coplanar and equiangular beams: 36°, 108°, 180°, 252° and 324°, in a 72 Gy plan. The dose–volume constraint used for the rectum and bladder was 70% of the volume receives >40% of the goal dose.

The second case is an oropharynx cancer planned using seven coplanar, but not equiangular, beams: 20°, 60°, 100°, 180°, 260°, 300° and 340°. This case has three CTVs; the prescribed doses for the gross disease region (CTVgr) and for the elective nodal regions (CTVel) were 74 Gy and 54 Gy, respectively. The dose–volume constraint for the spinal cord was maximum dose $\leqslant$ 45 Gy, and the constraint for both parotids was 50% of the volume receives >40% of the prescribed dose to the CTVgr.

The third case is a larynx cancer treated with a seven coplanar beam plan with beam angles, prescribed doses and constraints identical to the oropharynx case, with the exception of including three CTVel with the following prescribed doses: 66 Gy, 56 Gy and 50 Gy.

[5] The reduction ratio was selected starting from the minimum possible reduction of 50% (2:1) and increasing it (3:1, 4:1, etc) as long as the DVH remains similar to the original histogram using as criteria a change < 5% in D_{95} and D_{105} for the main target volume.

Table 1. NS and TNMU results for the original and the fixed NS plans (4:1 ratio). fNS = fixed NS, fMU = MU for fNS, %MU = MU reduction percentage.

	RP					OTNMU				
Beam	NS	fNS	MU	fMU	%MU	NS	fNS	MU	fMU	%MU
					(a) Prostate case					
36°	37	9	76	68	10.53	43	11	76	73	3.95
108°	29	7	97	79	18.56	29	7	97	61	37.11
180°	47	12	95	92	3.16	49	12	95	84	11.58
252°	25	6	82	63	23.17	27	7	82	67	18.29
324°	41	10	109	92	15.60	43	11	109	80	26.61
Total	179	44	459	394	14.16	191	48	459	365	20.48
					(b) Oropharynx case					
260°	28	7	49	30	38.78	30	8	49	45	8.16
300°	40	10	49	43	12.24	44	11	49	45	8.16
340°	51	13	68	55	19.12	53	13	68	54	20.59
20°	52	13	74	65	12.16	53	13	77	58	24.68
60°	32	8	38	29	23.68	27	7	38	30	21.05
100°	29	7	45	27	40.00	30	8	46	29	36.96
180°	46	12	55	51	7.27	45	11	56	49	12.50
Total	278	70	378	300	20.63	282	71	383	310	19.06
					(c) Larynx case					
260°	42	11	58	47	18.97	43	11	60	51	15.00
300°	53	13	66	57	13.64	55	14	67	55	17.91
340°	57	14	70	59	15.71	58	15	70	59	15.71
20°	43	11	66	55	16.67	43	11	66	53	19.70
60°	38	10	62	50	19.35	44	11	62	49	20.97
100°	58	15	85	72	15.29	59	15	85	66	22.35
180°	59	15	70	61	12.86	60	15	77	58	24.68
Total	350	89	477	401	15.93	362	92	487	391	19.71

Additionally, we planned ten cancer cases in different body locations for including the dosimetric index results obtained in the main target volume. In these cases, only the number of beams and the prescribed dose for the main target volume were included in table 5.

3. Results

In order to provide an example of the results achieved, we applied our method to the segmentation shown in figure 1, which corresponds to the 252° beam of the prostate case. The result can be seen in figure 3.

Table 1 summarizes the NS and TNMU results for the original and the processed plans. The columns referring to the latter have the prefix 'f' (meaning fixed). The NS reduction is not shown because it was 75% $\pm$ 0.67, whereas the MU reduction is explicitly reported since it was more variable. As an example of the time reduction achieved, the beam delivery times for the prostate and larynx cases, which had the smallest and biggest NS, are shown in table 2 for the RP. For the sake of brevity and conciseness, the results for the OTNMU

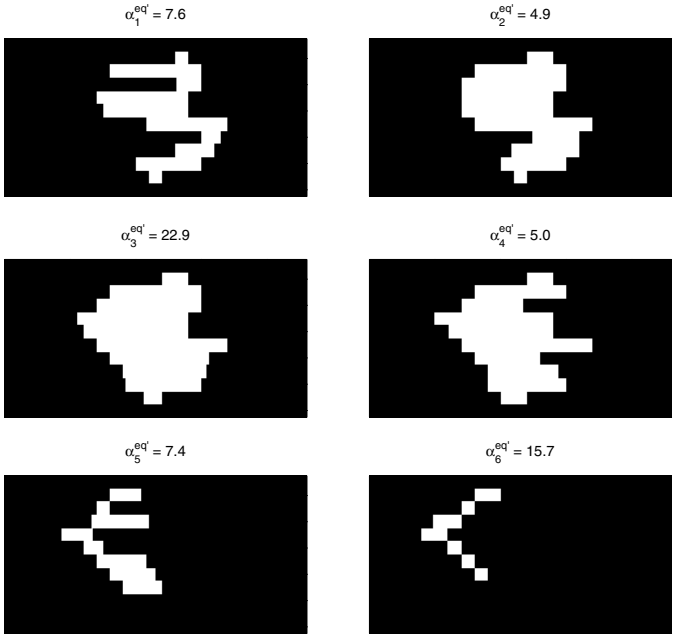

Figure 3. Prostate segmentation of figure 1 processed for obtaining six segments.

Table 2. Beam delivery time table (in mm:ss) for the rod pushing technique in the original and the fixed NS plans (4:1 ratio). Beam order is the delivery order. 'Trans' is the transition time spent from the previous beam to the current one. 'Rad' is the total beam delivery time (beam-on time plus the time required for the leaves to move between segments).

	Original		Fixed	
Beam	Trans	Rad	Trans	Rad
	(a) Prostate case			
180°	00:00	03:10	00:00	01:44
252°	00:26	02:04	00:30	01:02
324°	00:25	03:08	00:31	01:39
36°	00:25	02:35	00:25	01:19
108°	00:27	02:21	00:25	01:17
Total	01:43	13:18	01:51	07:01
	(b) Larynx case			
180°	00:00	02:44	00:00	01:15
100°	00:25	03:19	00:19	01:29
60°	00:19	03:29	00:19	01:27
20°	00:19	02:47	00:20	01:17
340°	00:21	02:41	00:19	01:17
300°	00:21	03:38	00:25	01:42
260°	00:29	03:38	00:28	01:32
Total	02:14	22:16	02:10	09:59

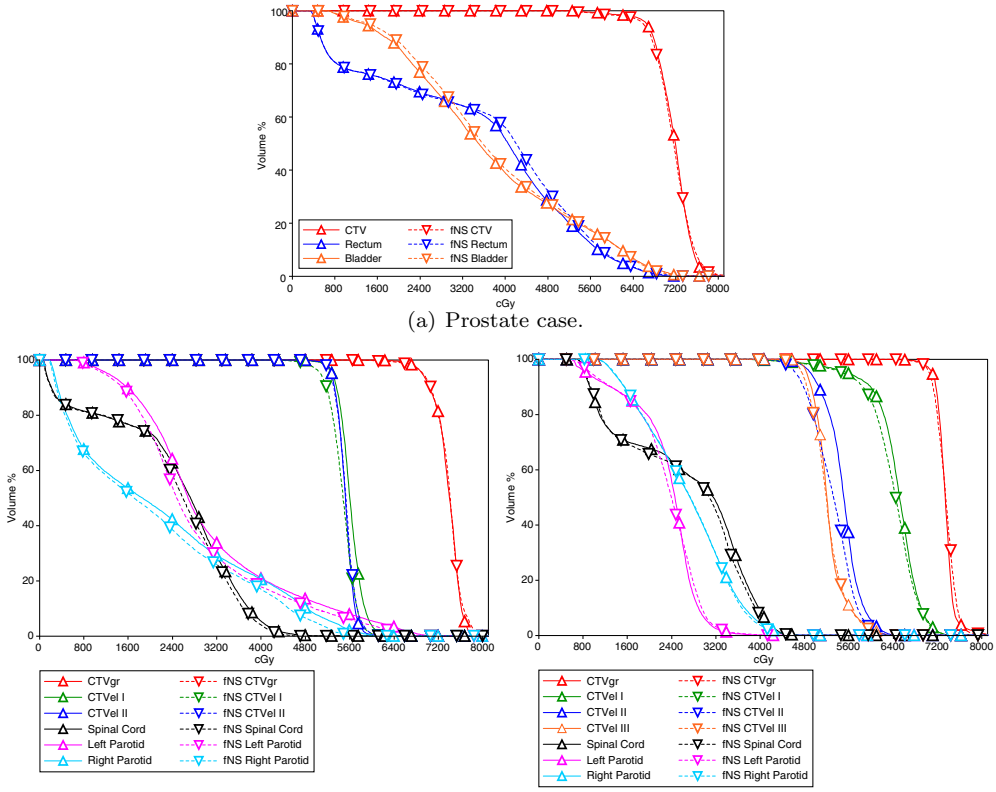

(a) Prostate case.

(b) Oropharynx case.

(c) Larynx case.

Figure 4. DVHs for the rod pushing algorithm. fNS = fixed NS.

algorithm are only presented in table 1, because they were very similar to those of the RP in the measurements.

The dosimetric comparison between each original plan and its corresponding processed plan was performed using a DVH. The DVHs for the three detailed cases are shown together in figure 4. In addition, we used the equivalent uniform dose (EUD), as described and implemented in Gay and Niemierko (2007), the D_{95} and the D_{100} indexes in order to quantify the dosimetric differences between both plans. The results of these indexes can be seen in table 3 together with the *a* parameter used in the EUD formula for each region of interest (ROI). Table 3(a) also includes a study of change in EUD, D_{95} and D_{100} as a function of the NS reduction for the prostate case. The ratios ranged from 2:1 to 6:1.

Additionally, we used the modulation index (MI) described in Webb (2003) for assessing how the complexity of the treatment plan varies between the original plan, with an unrestricted NS, and the fixed NS approach. The MI results are presented in table 4 for the original and the new fluence matrices. The latter was a reconstruction using the segmentation obtained from the proposed method and adjusting the leaves to the original beamlet positions with a round function, since this index was designed for discrete fluence matrices.

Lastly, table 5 provides the EUD, the D_{95} and the D_{100} dosimetric indexes for the main target volume in ten cancer cases using again a ratio of 4:1 for fixing the NS.

Table 3. Dosimetric index comparison between the original and the fixed NS plans (4:1 ratio) using the EUD, D_{95} and D_{100}. D_x is defined as the percentage of volume receiving x% of the prescribed dose.

(a) The EUD, D_{95} and D_{100} are included as a function of the NS reduction for the prostate case. The total NS for each plan is beside its ratio between brackets

ROI	Index	a	Original	2:1 (92)	3:1 (60)	4:1 (44)	5:1 (35)	6:1 (30)
CTV	EUD	−10	70.07 Gy	69.86 Gy	70.04 Gy	69.53 Gy	69.52 Gy	69.47 Gy
	D_{95}		85.72%	84.61%	85.42%	83.56%	80.04%	75.51%
	D_{100}		48.68%	44.15%	47.01%	45.21%	44.79%	45.97%
Rectum	EUD	6	48.00 Gy	47.98 Gy	48.86 Gy	48.82 Gy	49.55 Gy	50.26 Gy
Bladder	EUD	6	49.72 Gy	49.50 Gy	50.09 Gy	49.71 Gy	50.47 Gy	51.03 Gy

ROI	Index	a	Original	Fixed
	(b) Oropharynx case			
CTVgr	EUD	−10	73.20	72.92
	D_{95}		93.78	90.40
	D_{100}		49.00	46.65
CTVel I	EUD	−10	56.07	54.29
CTVel II	EUD	−10	55.04	54.37
Spinal cord	EUD	13	35.77	33.59
Left parotid	EUD	0.5	18.69	17.59
Right parotid	EUD	0.5	29.19	28.26
	(c) Larynx case			
CTVgr	EUD	−10	73.05	72.91
	D_{95}		97.58	93.37
	D_{100}		22.54	35.94
CTVel I	EUD	−10	60.51	59.23
CTVel II	EUD	−10	54.46	52.83
CTVel III	EUD	−10	52.41	51.12
Spinal cord	EUD	13	36.00	35.06
Left parotid	EUD	0.5	27.05	26.98
Right parotid	EUD	0.5	22.47	21.78

4. Discussion

The rationale behind the proposed method for reducing the NS is to provide the radiation oncologist the possibility of having some control over the NS obtained in two-phase step-and-shoot IMRT, as has been done in DSS or direct IMRT approaches based on class solutions and patient anatomy (Damen *et al* 2001, Arráns *et al* 2003).

For all the cases presented in section 3, we fixed the NS with a ratio of 4:1 for all beams, since this was the biggest reduction that did not considerably modify the DVHs using as criteria a change <5% in D_{95} and D_{105} for the main target volume. For the three cases reported in detail, the number of apertures obtained can be seen in table 1. These numbers are much closer to the results reported for DSS methods in similar cases (Jiang *et al* 2005, Dobler *et al* 2007, Carlsson 2008, Broderick *et al* 2009), which are between five and ten apertures

Table 4. Modulation index for each beam in the original and the fixed NS plans (4:1 ratio).

(a) Prostate case

Beam	Original	Fixed
36°	2.18	1.86
108°	2.08	1.63
180°	2.15	1.94
252°	2.33	2.19
324°	2.31	1.53
Average	2.21	1.83

(b) Oropharynx and Larynx cases

	Oropharynx		Larynx	
Beam	Original	Fixed	Original	Fixed
180°	5.18	3.11	6.00	5.06
100°	5.18	4.29	4.61	3.99
60°	4.24	3.39	5.40	4.05
20°	5.13	4.56	4.61	3.66
340°	5.72	4.64	5.09	4.85
300°	6.63	4.33	5.49	4.70
260°	5.60	4.33	5.60	4.64
Average	5.38	4.09	5.26	4.42

per beam, than to two-phase IMRT systems. The MI results in table 4 showed that there is also an important simplification of the fluence delivered and treatment complexity when using the fixed NS approach. In addition, the TNMU is reduced more than 14% in all cases, and this NS and TNMU reduction considerably decreases treatment times. As an example of the time-saving effect that can be achieved, the total delivery time for the RP technique, without taking into account beam transitions, is reduced by 47.2% for the prostate case and by 55.1% for the larynx case, as can be seen in table 2. These measurements were obtained using an Optifocus™ MLC with a negligible verification and recording cycle (V&R) overhead (no delays between segments, apart from the leaf travel time itself). This means that experiments were performed under the most unfavourable conditions, i.e. any MLC with a V&R $\geqslant$ 1 s can obtain greater time reductions.

The DVHs in figure 4 show that the method is able to reduce the original NS in our plans while (1) keeping the dose delivered to the main CTV close to its original one, (2) the OAR histogram curves are very similar and (3) the maximum dose delivered to OARs is never significantly increased. In addition, the EUD for each ROI and plan presented in table 3 also suggests that there are no substantial modifications, in dosimetric terms, between the original and the fixed NS approaches. Similar results can be seen in table 5 for the main target volume in ten cancer cases, where the difference in EUD between both plans is smaller than 1 Gy. The observed changes for D_{100} in table 5 are explained by the fact that the curve steepness is often slightly modified and the kind of normalization applied tends to preserve the D_{95} index. As a consequence, the D_{100} index is prone to suffer variations.

As expected, the larger the NS reduction for all the beams, the greater is the difference between the original and the final dose, as reported in table 3(a) for the prostate case. During

Table 5. Comparison of the EUD, D_{95} and D_{100} for the main target volume in ten additional cancer cases between the original and the fixed NS approaches (4:1 ratio).

ID	Location	Beams	Goal dose (Gy)	Approach	EUD (Gy)	D_{95} (%)	D_{100} (%)
1	Endometrium	6	18.00[a]	Original	16.62	85.90	54.61
				Fixed	16.03	83.19	50.67
2	Prostate	6	78.00	Original	77.33	91.61	55.63
				Fixed	77.11	88.06	57.42
3	Prostate	5	78.00	Original	76.70	96.27	5.61
				Fixed	76.29	92.03	19.11
4	Prostate	6	76.00	Original	75.96	97.70	59.17
				Fixed	75.57	93.97	54.67
5	Prostate	6	74.00	Original	72.38	93.32	18.86
				Fixed	72.22	88.18	25.89
6	Head-and-neck	7	68.40	Original	67.86	96.25	40.03
				Fixed	68.01	91.60	59.23
7	Head-and-neck	8	70.00	Original	69.40	90.71	57.15
				Fixed	68.72	86.05	45.86
8	Head-and-neck	6	66.00	Original	65.96	96.16	57.56
				Fixed	66.10	95.69	60.39
9	Pancreas	6	10.00[b]	Original	10.14	99.79	66.98
				Fixed	9.84	92.19	23.70
10	Pelvis and Sacrum	5	50.40	Original	52.44	99.89	97.92
				Fixed	53.21	99.82	95.56

[a] Twice a day, hyper-fractionation. [b] Re-irradiation.

the experimental stage we found that reductions beyond the ratio 5:1 may cause modifications in the DVH that would not be acceptable in many cases. We observed that this behaviour is due to the difficulty of representing with a single aperture a group with five segments or more, because the difference between the first segment and the last one within the group may be considerable.

5. Conclusions

The method presented in this work is able to reduce the NS in two-phase step-and-shoot IMRT treatment planning systems to an *a priori* fixed value. This NS reduction is computed by clustering the original segments into groups, and creating an equivalent segment with its associated weight for each group.

The results of the testing in clinical cases show that final segmentation with a reduction in the NS up to 75% obtained a DVH and dosimetric indexes very similar to the original ones, so the plan quality was not compromised. In addition, the TNMU was also decreased and both NS and TNMU reductions considerably shortened treatment times.

For our future research, we would like to extend our method for incorporating limitations or effects of MLCs such as field size, carriage splits, leaf rounding or tongue-and-groove and working with minimizing leaf travelling criteria other than unidirectionality.

Acknowledgments

The authors would like to thank the Physics and Radiological Protection Service staff at the Hospital Clínico Universitario Lozano Blesa and the Técnicas Radiofísicas SL company for their collaboration on the experiments. We would also like to thank the two anonymous referees for providing us with constructive comments and suggestions.

Appendix. Equivalent segment computation example

Example 1. The W weighting matrix is computed for a random fluence matrix and its unidirectional segmentation. The original segments (with their left and right leaves shaded in light and dark grey, respectively)

$$A = \begin{bmatrix} 0 & 2 & 4 \\ 1 & 2 & 1 \\ 2 & 4 & 1 \end{bmatrix} = \begin{bmatrix} 0 & 1 & 1 \\ 1 & 1 & 0 \\ 1 & 1 & 0 \end{bmatrix} + \begin{bmatrix} 0 & 1 & 1 \\ 0 & 1 & 0 \\ 1 & 1 & 0 \end{bmatrix} + \begin{bmatrix} 0 & 0 & 1 \\ 0 & 0 & 0 \\ 0 & 1 & 0 \end{bmatrix} + \begin{bmatrix} 0 & 0 & 1 \\ 0 & 0 & 1 \\ 0 & 1 & 1 \end{bmatrix}$$

are projected over the original fluence matrix A

$$\begin{bmatrix} 0 & 2 & 4 \\ 1 & 2 & 0 \\ 2 & 4 & 0 \end{bmatrix}; \begin{bmatrix} 0 & 2 & 4 \\ 0 & 2 & 0 \\ 2 & 4 & 0 \end{bmatrix}; \begin{bmatrix} 0 & 0 & 4 \\ 0 & 0 & 0 \\ 0 & 4 & 0 \end{bmatrix}; \begin{bmatrix} 0 & 0 & 4 \\ 0 & 0 & 1 \\ 0 & 4 & 1 \end{bmatrix},$$

and the weighting matrix is obtained applying equation (4)

$$W = \begin{bmatrix} 6 & 6 & 4 & 4 \\ 3 & 2 & 0 & 1 \\ 6 & 6 & 4 & 5 \end{bmatrix}.$$

Example 2. Let us assume that example 1 segmentation is reduced to two segments, and let us assume that the first group has three segments and the second group has the last segment. Accordingly,

$$A_1^{\mathrm{cu}} = \begin{bmatrix} 0 & 2 & 3 \\ 1 & 2 & 0 \\ 2 & 3 & 0 \end{bmatrix} = \begin{bmatrix} 0 & 1 & 1 \\ 1 & 1 & 0 \\ 1 & 1 & 0 \end{bmatrix} + \begin{bmatrix} 0 & 1 & 1 \\ 0 & 1 & 0 \\ 1 & 1 & 0 \end{bmatrix} + \begin{bmatrix} 0 & 0 & 1 \\ 0 & 0 & 0 \\ 0 & 1 & 0 \end{bmatrix}.$$

Then, the $S_1^{\mathrm{eq}'}$ equivalent segment is computed porting the segments to the continuous leaf position representation

$$\begin{bmatrix} 1.0 & 3.0 \\ 0.0 & 2.0 \\ 0.0 & 2.0 \end{bmatrix} + \begin{bmatrix} 1.0 & 3.0 \\ 1.0 & 2.0 \\ 0.0 & 2.0 \end{bmatrix} + \begin{bmatrix} 2.0 & 3.0 \\ 2.0 & 2.0 \\ 1.0 & 2.0 \end{bmatrix},$$

and applying equation (6) with example 1 weighting matrix

$$S_1^{\mathrm{eq}'} = \begin{bmatrix} 1.2 & 3.0 \\ 0.4 & 2.0 \\ 0.2 & 2.0 \end{bmatrix}.$$

References

Alber M and Nüsslin F 2000 Intensity modulated photon beams subject to a minimal surface smoothing constraint *Phys. Med. Biol.* **45** N49–52

Arráns R, Gallardo M I, Roselló J and Sánchez-Doblado F 2003 Computer optimization of class solutions designed on a beam segmentation basis *Radiother. Oncol.* **69** 315–21

Artacho J, Mellado X, Tobías G, Cruz S and Hernández M 2009 A novel unidirectional intensity map segmentation method for step-and-shoot IMRT delivery with segment shape control *Phys. Med. Biol.* **54** 569–89

Bär W, Alber M and Nüsslin F 2001 A variable fluence step clustering and segmentation algorithm for step and shoot IMRT *Phys. Med. Biol.* **46** 1997–2007

Broderick M, Leech M and Coffey M 2009 Direct aperture optimization as a means of reducing the complexity of intensity modulated radiation therapy plans *Radiat. Oncol.* **4** 8

Carlsson F 2008 Combining segment generation with direct step-and-shoot optimization in intensity-modulated radiation therapy *Med. Phys.* **35** 3828–38

Damen E M, Brugmans M J, van der Horst A, Bos L, Lebesque J V, Mijnheer B J, McShan D L, Fraass B A and Kessler M L 2001 Planning, computer optimization, and dosimetric verification of a segmented irradiation technique for prostate cancer *Int. J. Radiat. Oncol. Biol. Phys.* **49** 1183–95

Dobler B, Pohl F, Bogner L and Koelbl O 2007 Comparison of direct machine parameter optimization versus fluence optimization with sequential sequencing in IMRT of hypopharyngeal carcinoma *Radiat. Oncol.* **2** 33

Galvin J M, Chen X G and Smith R M 1993 Combining multileaf fields to modulate fluence distributions *Int. J. Radiat. Oncol. Biol. Phys.* **27** 697–705

Gay H A and Niemierko A 2007 A free program for calculating EUD-based NTCP and TCP in external beam radiotherapy *Phys. Med.* **23** 115–25

Hårdemark B, Liander A, Rehbinder H and Löf J 2003 Direct machine parameter optimization with RayMachine in Pinnacle *RaySearch White Paper* (Stockholm: RaySearch Laboratories AB)

Jiang Z, Earl M A, Zhang G W, Yu C X and Shepard D M 2005 An examination of the number of required apertures for step-and-shoot IMRT *Phys. Med. Biol.* **50** 5653–63

Löf J and Rehbinder H 2002 Inverse planning optimization with RayOptimizer in Pinnacle *RaySearch White Paper* (Stockholm: RaySearch Laboratories AB)

Matuszak M M, Larsen E W and Fraass B A 2007 Reduction of IMRT beam complexity through the use of beam modulation penalties in the objective function *Med. Phys.* **34** 507–20

Mellado X, Cruz S, Artacho J M and Canellas M 2010 Reducing the number of segments in unidirectional MLC segmentations *Phys. Med. Biol.* **55** N75–85

Romeijn H E, Ahuja R K, Dempsey J F and Kumar A 2005 A column generation approach to radiation therapy treatment planning using aperture modulation *SIAM J. Optim.* **15** 838–62

Sharpe M B, Miller B M, Yan D and Wong J W 2000 Monitor unit settings for intensity modulated beams delivered using a step-and-shoot approach. *Med. Phys.* **27** 2719–25

Shepard D M, Earl M A, Li X A, Naqvi S and Yu C 2002 Direct aperture optimization: a turnkey solution for step-and-shoot IMRT *Med. Phys.* **29** 1007–18

Siochi R A 1999 Minimizing static intensity modulation delivery time using an intensity solid paradigm *Int. J. Radiat. Oncol. Biol. Phys.* **43** 671–80

Spirou S V, Fournier-Bidoz N, Yang J, Chui C S and Ling C C 2001 Smoothing intensity-modulated beam profiles to improve the efficiency of delivery *Med. Phys.* **28** 2105–12

Webb S 2003 Use of a quantitative index of beam modulation to characterize dose conformality: illustration by a comparison of full beamlet IMRT, few-segment IMRT (fsIMRT) and conformal unmodulated radiotherapy *Phys. Med. Biol.* **48** 2051

Webb S, Convery D J and Evans P M 1998 Inverse planning with constraints to generate smoothed intensity-modulated beams *Phys. Med. Biol.* **43** 2785–94

Wu Y, Yan D, Sharpe M B, Miller B and Wong J W 2001 Implementing multiple static field delivery for intensity modulated beams *Med. Phys.* **28** 2188–97